Particulate levodopa nose-to-brain delivery targets dopamine to the brain with no plasma exposure

Savvas Dimiou[a,b], Rui M. Lopes[a,b], Ilona Kubajewska[a,b], Ryan D. Mellor[a,b], Corinna S. Schlosser[a,b], Manjunath S. Shet[c], Hugh Huang[c], Ozgur Akcan[c], Garth T. Whiteside[c], Andreas G. Schätzlein[a,b], Ijeoma F. Uchegbu[a,b*]

[a] *UCL School of Pharmacy, 29-39 Brunswick Square, London WC1N 1AX, UK*

[b] *Nanomerics Ltd., 6th Floor, 2 London Wall Place, London EC2Y 5AU, UK*

[c] *Imbrium Therapeutics, One Stamford Forum, 201 Tresser Blvd., Stamford, CT 06901, USA*

***Corresponding Author:**

Prof. Ijeoma F. Uchegbu

Email address: ijeoma.uchegbu@ucl.ac.uk

Abstract

Levodopa (L-DOPA) is an oral Parkinson's Disease drug that generates the active metabolite - dopamine (DA) *in vivo*. However, oral L-DOPA exhibits low oral bioavailability, limited brain uptake, peripheral DA-mediated side effects and its poor brain bioavailability can lead to long-term complications. Here we show that L-DOPA forms stable (for at least 5 months) 300 nm nanoparticles when encapsulated within N-palmitoyl-N-monomethyl-N,N-dimethyl-N,N,N-trimethyl-6-O-glycolchitosan (GCPQ). A nano-in-microparticle GCPQ-L-DOPA formulation (D_{50} = 7.2 μm), prepared by spray-drying, was stable for one month when stored at room and refrigeration temperatures and was capable of producing the original GCPQ-L-DOPA nanoparticles upon aqueous reconstitution. Nasal administration of reconstituted GCPQ-L-DOPA nanoparticles to rats resulted in significantly higher DA levels in the brain (C_{max} of 94 ng g^{-1} above baseline levels 2 hours post-dosing) when compared to nasal administration of L-DOPA alone, with DA being undetectable in the brain with the latter. Furthermore, nasal GCPQ-L-DOPA resulted in higher levels of L-DOPA in the plasma (a 17-fold increase in the Cmax, when compared to L-DOPA alone) with DA undetectable in the plasma from both formulations. These data provide evidence of effective delivery of DA to the brain with the GCPQ-L-DOPA formulation.

Keywords

GCPQ, Nano-in-microparticles, Chitosan, Levodopa, Nose-to-brain, Parkinson's Disease

1. Introduction

The incidence of neurodegenerative disorders is expected to increase significantly in the twenty-first century due to increases in lifespan (Sharma, Lohan et al. 2014). Parkinson's disease (PD), the second most common neurodegenerative disorder, is characterised by cardinal motor features, such as bradykinesia, rigidity, postural inability, and resting tremor (Olanow, Stern et al. 2009). PD's prevalence increases with age, affecting 2% and 5% of persons aged over 65 and 85 respectively (Tambasco, Romoli et al. 2018). PD occurs primarily due to the loss of dopaminergic pigmented neurons (dopamine-producing cells) in the substantial nigra (SN) pas compacta; thus, leading to dopamine deficiency (zhou, Liu et al. 2020). In the SN of a healthy brain, the only available pathway for dopamine (DA) production is via the metabolism of L-3,4-dihydroxyphenylalanine (L-DOPA); the latter of which is derived from the hydroxylation of tyrosine. Nevertheless, in a diseased brain, the SN cells are depleted leading to DA deficiency in striatal cells (Tambasco, Romoli et al. 2018). Although the exact cause for neuronal death in PD is unknown, many cellular mechanisms are believed to be responsible such as proteasomal and mitochondrial dysfunction (Pardeshi, Belgamwar et al. 2013).

PD treatment with administration of external DA is limited as DA cannot enter the brain due to its poor blood brain barrier (BBB) penetration (Melamed, Hefti et al. 1980, Rautio, Kumpulainen et al. 2008). Various drugs are employed to treat the disease, however, the ''gold standard'' therapy for PD, is the administration of L-DOPA, the direct precursor of DA (Sharma, Lohan et al. 2014). L-DOPA crosses the BBB to some extent reaching the central nervous system (CNS), where it is converted to DA and provides robust relief from the motor signs and symptoms of PD (Blandini and Greenamyre 1999, Olanow, Stern et al. 2009). Nevertheless, L-DOPA has low oral bioavailability (30%) and it undergoes extensive metabolism in the peripheral circulation by aromatic L-amino acid decarboxylase (AAADC) thus limiting brain uptake (Contin, Riva et al. 1996). Thus, to achieve the desired concentration at the target tissue, a higher dose of L-DOPA is administered leading to common short-term side effects such as nausea, hypertension, and hallucinations (Hamsaraj and Ramachandra Murthy Rayasa 1970, Gabathuler 2010, Abbott 2013, Gao 2016). Co-administration of L-DOPA and carbidopa, a peripheral amino acid decarboxylase inhibitor, prevents peripheral degradation and consequently increases the amount of L-DOPA in the

systemic circulation alleviating some of the short-term side effects (Sharma, Lohan et al. 2014, Haddad, Sawalha et al. 2017). Although the oral route is preferable for the management of chronic diseases such as PD, the highly variable absorption of L-DOPA due to erratic/delayed gastric emptying, as well as the competition for absorption and transport into the brain with other large neutral amino acids, hinders it from being as effective a treatment as it could be (Wade, Mearrick et al. 1973, Leenders, Poewe et al. 1986). Furthermore, the aforementioned issues associated with the oral delivery of L-DOPA can lead to long-term complications such as motor fluctuations and dyskinesias (Tolosa, Martí et al. 1998, Patel and Jimenez-Shahed 2018). Thus, there is an unmet medical need for an efficient delivery system able to avoid these long-term complications by improving the therapeutic efficacy of L-DOPA and providing higher drug bioavailability to the brain.

In recent years, the transport of exogenous materials directly from nose-to-brain as a potential route to bypass the BBB has been reported (Arisoy, Sayiner et al. 2020). The intranasal administration of drugs has the potential to prevent peripheral degradation, eliminate the drawbacks associated with oral administration, and allow targeted delivery to the site of action, the brain (Brime, Ballesteros et al. 2000, Seju, Kumar et al. 2011, Godfrey, Iannitelli et al. 2018, Pires and Santos 2018). The use of colloidal carriers, such as nanoparticles, is a promising strategy to achieve brain drug delivery through intranasal administration (Wu, Hu et al. 2008). Nevertheless, the major limitation of intranasal drug administration is the removal of nanoparticles by nasal drainage before the formulation has been sufficiently absorbed (Arisoy, Sayiner et al. 2020).

We have previously shown the delivery of a low molecular weight and metabolically labile peptide, leucine^{5} -enkephalin (LENK), exclusively to the brain formulated as nanoparticles after intranasal administration to rats with no peripheral exposure or activity (Godfrey, Iannitelli et al. 2018). This nanoparticulate LENK formulation utilises our biocompatible, mucoadhesive self-assembling polymer N-palmitoyl-N-monomethyl-N,N-dimethyl-N,N,N-trimethyl-6-O-glycolchitosan (GCPQ), which has also been shown to enhance the oral bioavailability of hydrophilic and hydrophobic molecules (Lalatsa, Garrett et al. 2012, Siew, Le et al. 2012, Godfrey, Iannitelli et al. 2018). Furthermore, GCPQ has proven to be non-toxic via the nasal route by a Good Laboratory Practice (GLP) toxicology screen (Godfrey, Iannitelli et al. 2018) (Pyrć, Milewska et al. 2020).

In the present study, we expand on our previous work on GCPQ to investigate whether L-DOPA-loaded GCPQ nano-in-microparticles can efficiently deliver L-DOPA to the brain and in turn induce the formation of its active metabolite, DA, after intranasal administration. While L-DOPA delivery to the brain *via* the intranasal route has been inferred by others (Chun, Lee et al. 2011, Sharma, Lohan et al. 2014, Nedorubov, Pavlov et al. 2019, Arisoy, Sayiner et al. 2020); here we demonstrate the preparation of an L-DOPA dry powder nano-in-microparticulate dosage form for intranasal administration. While not the subject of the present work, this formulation in combination with an appropriate nasal delivery device, such as our Naltos delivery device (Wang, Xiong et al. 2019), may indeed prove advantageous for the delivery of nasal L-DOPA to humans.

2. Materials and methods

2.1. Materials

All reagents and chemicals were obtained from Sigma-Aldrich Chemical Co., Poole, UK, unless otherwise stated. All solvents and acids were obtained from Fisher Scientific, Loughborough, UK. GCPQ was supplied by Nanomerics Ltd (Lot Number = 20180530-RM-GCPQ-01). L-DOPA was supplied by Ajinomoto Co., Inc., Tokyo, Japan. Deuterated L-DOPA (L-DOPA-d_3) was supplied by Cayman Chemicals, Cambridge, UK. Milli-Q water was used to prepare mobile phases and all other aqueous solutions.

2.2. Methods

2.2.1. Preparation of GCPQ-L-DOPA nanoparticles

GCPQ-L-DOPA nanoparticles were prepared from GCPQ (40 mg mL^{-1}, 0.5 mL) and L-DOPA (3 mg mL^{-1}, 1.34 mL) by vigorous mixing for 5 minutes followed by probe sonication (MSE Soniprep 150, MSE London, UK) for 1 minute on ice with the instrument set at an amplitude of 7. GCPQ-L-DOPA formulations for intranasal administration had a GCPQ, L-DOPA weight ratio of 10:2. GCPQ-L-DOPA nanoparticles were also lyophilised overnight after the addition of the cryoprotectant, sucrose (8.15 mg mL^{-1}), at a GCPQ, L-DOPA, sucrose weight ratio of 10: 2: 7.5.

2.2.2. Preparation of GCPQ-L-DOPA nano-in-microparticles

GCPQ-L-DOPA nanoparticles were prepared from GCPQ (50 mg mL^{-1}) and L-DOPA (3 mg mL^{-1}) in distilled water (26.67 mL) at a total solid concentration of 1.4% w/v and a GCPQ, L-DOPA mass ratio of 10: 2. The resulting nanoparticle dispersion was spray-dried to give GCPQ-L-DOPA nano-in-microparticles (Büchi Nano Spray Dryer B290, Büchi Labortechnik AG, Switzerland, inlet temperature = 130°C, outlet temperature = 65-75°C, aspirator rate = 35 m^3 h^{-1}, spray rate = 3 mL min^{-1}, gas flow = 357 L h^{-1}). The yield was 400 mg and the % yield was 83.3%.

2.2.3. Characterisation of GCPQ-L-DOPA nanoparticles and GCPQ-L-DOPA nano-in-microparticles

2.2.3.1. L-DOPA analysis

L-DOPA analysis was performed by high performance liquid chromatography (HPLC) (1220 Infinity II LC Gradient System, Agilent Technologies, UK). L-DOPA analysis was performed by UV detection at a fixed wavelength of 280 nm. Separation and quantification were carried out in a Synergi^{TM} Polar-RP analytical column (4 µm particle size, 4.6 mm x 250 mm, 80Å, Phenomenex, UK) eluted with a mobile phase consisting of water, acetonitrile, trifluoroacetic acid (94.99: 5: 0.01 (v/v)) at a flow rate of 1 mL min^{-1} (column temperature = 30°C, injection volume = 10 µL, calibration curve for quantification: y = 11.676x + 1.143, r^2 = 0.999, calibration curve range = 1.6-200.0 µg mL^{-1}, n = 4 separate experiments, retention time for L-DOPA = 3.9 min, total run time = 10 min). Data analysis was performed *via* Agilent Chemstation.

GCPQ-L-DOPA nano-in-microparticles were dispersed in water and mixed for 30-45 seconds to regenerate nanoparticles to a final concentration of 8 mg mL^{-1} of L-DOPA (unless otherwise stated). The L-DOPA content in all formulations was quantified in the supernatant after centrifugation (2,500 rpm for 2 minutes, Biofuge Fresco, Thermo Scientific, Sweden) to remove any non-encapsulated drug. An aliquot of the supernatant (50 µL) was diluted 20 times with the mobile phase and the solution injected on to the column for analysis. L-DOPA loading was calculated using the following formula:

$$L - DOPA\ Loading = \frac{(L-DOPA\ in\ supernatant)}{Total\ L-DOPA} \text{ x } 100$$

All standards were diluted in the mobile phase prior to analysis by HPLC. The method was validated with respect to linearity, accuracy, precision, limit of quantification (LOQ) and detection (LOD). Assay validation parameters appear in the Supplementary Information (Table S1).

2.2.3.2. Nanoparticle size and surface charge

The particle size of GCPQ-L-DOPA nanoparticles was determined using dynamic light scattering (DLS; Zetasizer Nano ZS, Malvern Instruments, UK) at a scattering angle of 173°, a temperature of 25°C, and a wavelength of 633 nm. Samples containing ~ 8 mg mL^{-1} L-DOPA were diluted 10 times with water and measurements were performed on the diluted samples. Three measurements were performed on each sample and a mean and standard deviation were reported as well as the polydispersity index (PDI). The surface charge of GCPQ-L-DOPA nanoparticles was determined using a Zetasizer Nano ZS. Samples containing ~ 8 mg mL^{-1} L-DOPA were diluted 10 times with water and loaded into zeta potential cuvettes (DTS1070, Malvern Instruments, UK).

2.2.3.3. Microparticle size distribution

The microparticle size distribution of the spray-dried GCPQ-L-DOPA nano-in-microparticles was determined by laser scattering using a Malvern Mastersizer 3000 (Malvern Instruments Ltd, Worcestershire, UK). An aliquot of the powder (~ 10 mg) was applied to the sample feeding tray. Air was used as the dispersion medium for the microparticles from the sample feeding tray to the sample cell. The microparticle size distribution of GCPQ-L-DOPA was characterised by the D_{10}, D_{50}, and D_{90}.

2.2.3.4. Morphology studies with scanning electron microscopy (SEM)

A strip of double-sided carbon tape was placed on an SEM stub (TAAB Laboratories Equipment Ltd, UK). GCPQ-L-DOPA nano-in-micro formulations were spread across the surface of the

tape and compressed air was used to remove loose microparticles. Samples were coated with a 20 nm gold sputter (Quorum Q150T, UK) before measurement. A Quanta 200F field emission SEM (ThermoFisher, The Netherlands) connected to a secondary electron detector (Everheart-Thomley Detector-ETD) was used to generate SEM images of the samples.

2.2.4. Stability of GCPQ-L-DOPA formulations

An aliquot of the GCPQ-L-DOPA nanoparticle formulation (3 mg mL^{-1} L-DOPA, 40 mg mL^{-1} GCPQ, 1.94 mL) was lyophilised (Christ Alpha 1-2 Ldplus, Martin Christ, Germany). Lyophilised GCPQ-L-DOPA formulations (n = 3 separate experiments) were stored in glass vials at room temperature (RT, 16 - 25°C), 4°C, and -30°C for 5 months. Spray-dried GCPQ-L-DOPA formulations (n = 3 separate experiments) were stored in glass vials at RT and 4°C for 1 month. At predetermined timepoints spray-dried GCPQ-L-DOPA nano-in-microparticles were characterised for their morphology and microparticle size distribution as described in sections 2.2.4.3-2.2.4.4. Furthermore, lyophilised and spray dried GCPQ-L-DOPA formulations were resuspended to 8 mg mL^{-1} of L-DOPA to evaluate L-DOPA loading, nanoparticle size, and surface charge as described in sections 2.2.4.1-2.2.4.2.

2.2.5. Animal studies

Adult male Sprague Dawley rats (Hilltop Animal Labs, Inc., Pennsylvania, USA; weight = 280 – 320 g) were housed (one and three per cage for cannulated and non-surgery rats respectively) in an air-conditioned unit (20–22°C, 50–60% humidity) and allowed free access to standard rodent chow and water. Lighting was controlled on a twelve-hour cycle (on at 07.00 h and off at 19.00 h). Animals were habituated for 7 days prior to experimentation and acclimatised to the procedure room for one hour prior to testing. All protocols were approved by a local institutional animal care and use committee (IACUC) and were carried out in accordance with the National Institutes of Health guide for the care and use of Laboratory animals (NIH Publications No. 8023, revised 1978). All animals were randomised by weight. Food was withheld from the animals for a minimum of twelve hours prior to dose administration until four hours post-dose and water was offered *ad libitum*. The in-life portion of the study was carried out at Absorption Systems LLC, Exton, PA, USA.

Prior to dosing, GCPQ-L-DOPA nano-in-microparticles and L-DOPA crystalline powder were dispersed in water to obtain a final concentration of 8 mg mL^{-1} of L-DOPA. As L-DOPA has an aqueous solubility of 3.3 mg mL^{-1} (Polanowska, Łukasik et al. 2019); after hydration crystal L-DOPA was a cloudy suspension, while the resuspended GCPQ-L-DOPA was a clear solution. The intranasal dose utilised was 1.2 mg kg^{-1}, which, depending on the animal weight, ranged between 20-25 µL of administration volume per nare (~0.15 mL kg^{-1}) and was administered using a pipette. Animals were anesthetised intramuscularly with ketamine HCl/ Xylazine HCl solution prior to dosing either a dispersion of GCPQ-L-DOPA or crystalline L-DOPA intranasally into both nares. At various timepoints, animals were euthanised for brain collection. Brains were removed, and brain tissue samples were rinsed with saline, patted dry, and weighed. Samples were then placed into chilled tubes and stored frozen until extraction. To each gram of brain tissue, 2 mL of methanol, water (20:80) was added. Samples were homogenised on ice using a Virsonic 100 ultrasonic homogenizer and stored frozen until analyses could be performed. Blood samples were taken either on termination by cardiac puncture or non-terminally via a jugular vein cannula and collected into K_2EDTA vacutainer tubes. Plasma was separated by centrifugation (3,000 g for 5 minutes at 4°C), treated with 25% sodium metabisulfite at a 10:1 ratio and stored frozen until analyses could be performed. The internal standard, L-DOPA-d_3, was prepared at 5 µg mL^{-1} and was diluted to 1 µg mL^{-1} during sample processing.

To 0.05 mL of rat brain homogenate or rat plasma, 0.01 mL of water and 0.15 mL of ice cold perchloric acid (2M) containing the internal standard L-DOPA-d_3 (1 µg mL^{-1}) were added. The mixtures were centrifuged (13,000 RPM for 10 minutes at 4°C) and the supernatants transferred to a clean 96-well plate and analysed by liquid chromatography with tandem mass spectrometry (LC-MS/MS). The values retrieved were converted in the relative concentrations (ng mL^{-1} for plasma and ng g^{-1} for brain) depending on the specific weight of the brain tissue and based on the constructed calibration curves as detailed below.

For the brain calibration curve, rat brain homogenate samples (0.05 mL) were mixed with water (0.01 mL), ice cold 2N perchloric acid spiked with L-DOPA-d_3 (1 µg mL^{-1}) and various concentrations of L-DOPA or DA to construct a standard curve after extraction (L-DOPA = 10 – 1000 ng mL^{-1}, L-DOPA-d_3 = 1000 ng mL^{-1}, $y = 0.000176x + 0.000452$, $r^2 = 0.9968$, DA = 10 – 1000 ng mL^{-1}, L-DOPA-d_3 = 1000 ng mL^{-1}, $y = 0.000217x + 0.00877$, $r^2 = 0.9947$).

For the plasma calibration curve, plasma samples (0.05 mL) were mixed with water (0.01 mL), ice cold 2N perchloric acid spiked with L-DOPA-d_3 (1 µg mL^{-1}) and various concentrations of L-DOPA or DA to construct a standard curve after extraction (L-DOPA = 10 – 1000 ng mL^{-1}, L-DOPA-d_3 = 1000 ng mL^{-1}, y= 0.000945x - 0.00051, r^2 = 0.9894 , DA = 10 – 1000 ng mL^{-1}, L-DOPA-d_3 = 1000 ng mL^{-1}, y= 0.000176x + 0.00764, r^2 = 0.9952).

LC-MS/MS analysis was carried out using a Waters Acquity UPLC system interfaced directly with a Sciex API 4000 triple quadrupole at Absorption Systems LLC, Exton, PA, USA. Samples were separated on a Waters Acquity BEH C18 column (1.7 µm particle size, 2.1 mm x 100mm) in a gradient mode with formic acid (FA; 0.1% w/v), methanol: t_0 = 99.5% FA, $t_{1.2}$ = 99.5% FA, t_2 = 1% FA, $t_{2.1}$ = 99.5% FA, $t_{3.5}$ = 99.5% FA. Mobile phase flow rate = 0.4 mL min^{-1}, column temperature = 40°C, injection volume = 10 µL, run time = 3.5 min. The retention times for L-DOPA, L-DOPA-d_3, and DA were 1.18 min, 1.16 min, and 1.22 min respectively. The samples were ionized by electrospray ionization (ESI) in a positive ion mode and by using the multiple reaction monitoring (MRM) mode as the ion detection mode. The optimal source parameters were as follows: collision-activated dissociation gas (CAD) 10 psi, curtain gas (CUR) 30 psi, nebuliser gas (gas 1) 50 psi, heater gas (gas 2) 50 psi, and source temperature 500°C. The compound dependent parameters are shown in Table 1.

Table 1. LC-MS/MS analytical conditions.

Name	Precursor ion	Product Ion	Declustering Potential (DP)*	Entrance Potential (EP)*	Collision Energy (CE)*	Collision Cell Exit Potential (CXP)*	Polarity
L-DOPA	198.1	152.1	60	10	20	7	Positive
DA	154.1	91.1	50	10	15	7	Positive
L-DOPA-d_3	200.1	154.1	30	10	20	12	Positive

*All settings are in Volts.

Representative LC-MS/MS spectra of L-DOPA, DA, and L-DOPA-d_3 from the rat plasma and brain calibration curves and from the rat pharmacokinetic study appear in the Supplementary Information (Figures S1-S4).

2.2.6. Statistical analysis

Data were expressed as means ± standard error of the mean (SEM) unless otherwise stated. The differences between means of two groups were compared by two-tailed unpaired Student's t-test or two-tailed unpaired Student's t-test with Welch's correction (where the assumption of populations' equal variances was not satisfied, as tested by the F-test). Comparisons of more than two groups were performed using ordinary one-way ANOVA followed by Dunnett's multiple comparisons test or non-parametric Kruskal-Wallis test followed by Dunn's multiple comparisons test (where the ANOVA assumption of normal data distribution was not satisfied, as revealed by the Brown-Forsythe test). Statistical significance was reported as P-values, with the following thresholds: *P < 0.05, **P < 0.01, ***P < 0.001, ****P < 0.0001. All statistical analyses were conducted using the GraphPad Prism (version 8.4.2) for Windows, GraphPad Software, San Diego, California, USA.

3. Results and discussion

3.1. GCPQ-L-DOPA nanoparticles

Formulation optimisation of GCPQ-L-DOPA nanoparticles was conducted on the basis of drug encapsulation. Process parameters such as mixing time, and probe sonication time were fixed at 5 minutes and 1 minute respectively. GCPQ and L-DOPA were mixed at various mass ratios, lyophilised, resuspended in water, centrifuged to remove unencapsulated drug and the drug loading was measured in the formulations' supernatant at various timepoints. Results from the optimisation experiments (data not shown) indicated that the GCPQ: L-DOPA mass ratio of 10: 2 gave the most suitable drug loading (95%; 7.5 mg mL^{-1} L-DOPA concentration) and was stable for up to 4 hours after reconstitution of the lyophilised formulations (Figure 1).

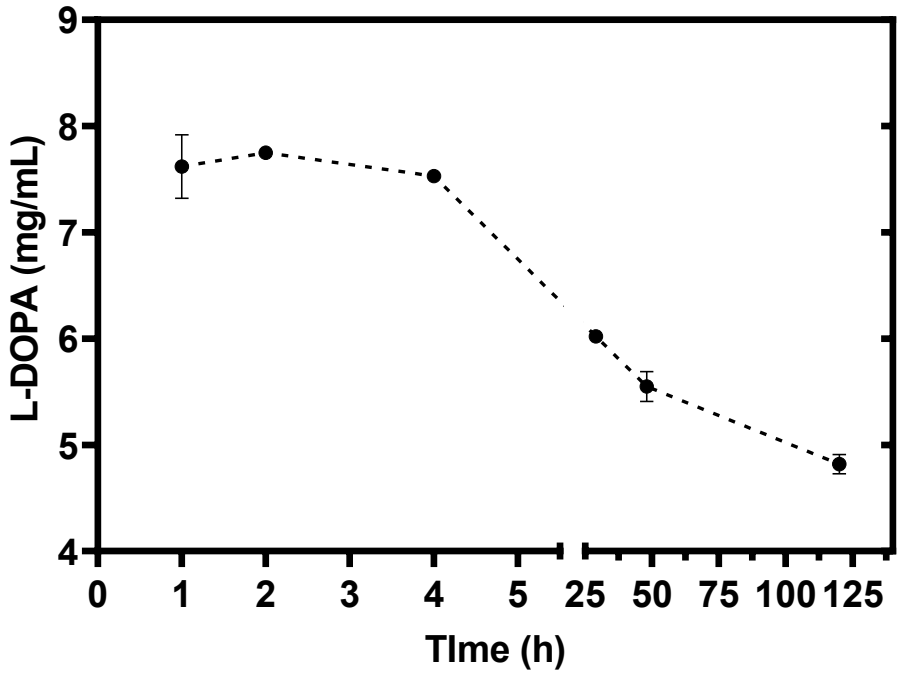

Figure 1. L-DOPA concentration (mg mL^{-1}) after reconstitution of the lyophilised GCPQ-L-DOPA formulation prepared at a GCPQ, L-DOPA mass ratio of 10:2 to 8 mg mL^{-1} L-DOPA (n= 3, mean ± SD).

The usual nasal administration volume in humans is between 100 – 200 µL and less than 1% of unchanged drug reaches cerebral circulation after administration (Kim, Kang et al. 2009). Thus, a vehicle with a solubility of at least 10 mg mL^{-1} of L-DOPA is needed. L-DOPA has an aqueous solubility of 3.3 mg mL^{-1} and is classified as a poorly soluble drug in water (Abbott 2010, Polanowska, Łukasik et al. 2019). Furthermore, solutions of L-DOPA are rapidly oxidised by atmospheric oxygen which leads to its degradation as observed by darkening of the solution (Stocchi, Ruggieri et al. 1989). Here we show that by utilising GCPQ and L-DOPA at the optimal GCPQ, L-DOPA mass ratio of 10:2 we produce a stable formulation with increased drug content (7.5 mg mL^{-1}). The optimised 10:2 formulation was stable for up to 4 hours after reconstitution retaining a high drug loading (95%). Due to L-DOPA's low water solubility, the quantities needed for a therapeutic effect via the nasal and oral route are substantial leading to irritation of the soft tissues (Abbott 2010). Furthermore, as the disease progresses, the L-DOPA dosing frequency needs to increase to maintain therapeutic benefit with prolonged use leading to severe peripheral side effects (Zahoor, Shafi et al. 2018). Thus, minimising the dose needed for therapeutic action by enabling increased dopamine brain bioavailability could alleviate some of these side effects.

The nanoparticle size and surface charge of the optimised GCPQ-L-DOPA formulation are presented in Table 2. L-DOPA is formulated with GCPQ into a mixture of 20 – 30 nm and 260 – 280 nm nanoparticles with a high positive surface charge of 40.5 mV. Furthermore, the nanoparticle size was not affected by the lyophilisation process with GCPQ-L-DOPA formulations presenting a bimodal particle size distribution with a main peak (peak 1) at 260 – 280 nm (70-75% of the intensity) and a secondary peak (peak 2) at 20 – 30 nm (25-30% of the intensity). The DLS analysis of the GCPQ-L-DOPA nanoparticles before and after lyophilisation as well as the GCPQ polymer alone appear in the Supplementary Information (Figure S5). Depending on the drug being encapsulated, GCPQ-drug formulations present as bimodal distributions comprising presumably empty polymeric micelles and micellar clusters/ drug filled particles (Qu, Khutoryanskiy et al. 2006).

Table 2. Physicochemical properties of L-DOPA and the GCPQ-L-DOPA 10:2 formulation before and after lyophilisation (n= 3, mean ± SD, ND = not determined).

Formulation	Z-Average (nm)	Peak 1 by size (nm) and intensity (% intensity)	Peak 2 by size (nm) and intensity (% intensity)	Zeta potential (mV)	PDI
GCPQ-L-DOPA before lyophilisation	76.0 ± 11.0	264 ± 36 (68 ± 6%)	26 ± 4 (29 ± 5%)	ND	0.91 ± 0.17
GCPQ-L-DOPA after lyophilisation	72.0 ± 5.0	283 ± 63 (73 ± 4%)	27 ± 7 (21 ± 4%)	40.5 ± 2.1	1.00 ± 0.00

GCPQ confers a highly positive surface charge (40.5 mV) on the nanoparticles. Positively or negatively charged polymers are known to bind to biological surfaces when compared to non-ionic polymers (Bruschi, de Souza Ferreira et al. 2020) and GCPQ nanoparticles are known to adhere to and integrate into intestinal mucosal surfaces (Siew, Le et al. 2012) and present with a prolonged residence time in the nares of rodents (Pyrć, Milewska et al. 2020) the latter

presumably due to the nasal mucoadhesion of GCPQ. Thus, we hypothesize that mucoadhesion may enhance the residence time of L-DOPA in the nares after intranasal administration of GCPQ-L-DOPA and in this way improve the brain bioavailability via the nasal route.

Physical stability of the lyophilised GCPQ-L-DOPA (mass ratio = 10:2) formulations was determined over a 5-month period of storage at -30°C, 4°C, and RT by examining key parameters such as drug loading, nanoparticle size, and nanoparticle surface charge as shown in Table 3. At each timepoint a sample of the lyophilised formulation was resuspended in water and the aforementioned parameters were measured.

Table 3. Stability parameters of lyophilised GCPQ-L-DOPA 10:2 formulations stored at -30°C, 4°C, and RT conditions for 5 months (n= 3, mean ± SD).

Formulation (Time)	L-DOPA concentration (mg mL^{-1}) and encapsulation efficiency	Z-average (nm)	Peak 1 by size (nm) and intensity (% intensity)	Peak 2 by size (nm) and intensity (% intensity)	Zeta potential (mV)	PDI
GCPQ-L-DOPA (0 month)	7.51 ± 0.06 (95%)	140 ± 14	289 ± 22 (84 ± 3%)	19 ± 3 (12 ± 2%)	40.1 ± 2.5	0.670 ± 0.141
GCPQ-L-DOPA -30°C (5 months)	7.45 ± 0.32 (93%)	127 ± 59	298 ± 44 (72 ± 9%)	21 ± 8 (20 ± 7%)	32.1 ± 3.5	0.820 ± 0.187
GCPQ-L-DOPA 4°C (5 months)	7.17 ± 0.57 (90%)	167 ± 20	292 ± 26 (84 ± 3%)	18 ± 3 (10 ±2%)	28.5 ± 4.2	0.614 ± 0.152
GCPQ-L-DOPA RT (5 months)	7.15 ± 0.73 (89%)	128 ± 48	308 ± 52 (67 ± 10%)	23 ± 5 (22 ± 9%)	31.1 ± 5.0	0.664 ± 0.252

As shown in Table 3, the lyophilised GCPQ-L-DOPA (mass ratio = 10:2) formulation was stable when stored at different storage temperatures. GCPQ was able to maintain L-DOPA stably

encapsulated at all storage conditions for at least five months, with only a small reduction (2-6%) in L-DOPA loading. Resuspended formulations presented a bimodal particle size distribution with a main peak at 260 – 280 nm (70-75% of the intensity) and a secondary peak at 20 – 30 nm (20-25% of the intensity) that was maintained for up to 5 months storage. Although particle surface charge had minor reductions throughout the stability study, it remained highly positive (>25 mV) for up to 5 months regardless of the storage conditions.

3.2. GCPQ-L-DOPA nano-in-microparticles

GCPQ-L-DOPA microparticles were prepared by spray drying the GCPQ-L-DOPA (mass ratio = 10:2) formulation. The spray dryer settings were optimised to increase the yield of the recovered GCPQ-L-DOPA microparticles (volume mean diameter = 6.15 µm, D_{10} = 2.19 ± 0.41, D_{50} = 5.27 ± 0.78, D_{90} = 11.0 ± 1.48). The parameters D10, D50 and D90 provide valuable size distribution insight with respect to the breadth of the microparticle size range and could reveal the presence of possible potential particle aggregates. These values reflect the diameter of the particles where either 10%, 50% or 90% of the population lies below a certain size (Maguire, Rösslein et al. 2018). L-DOPA crystals (as supplied by manufacturer) and GCPQ-L-DOPA nano-in-microparticles were analysed by SEM, as shown in Figure 2.

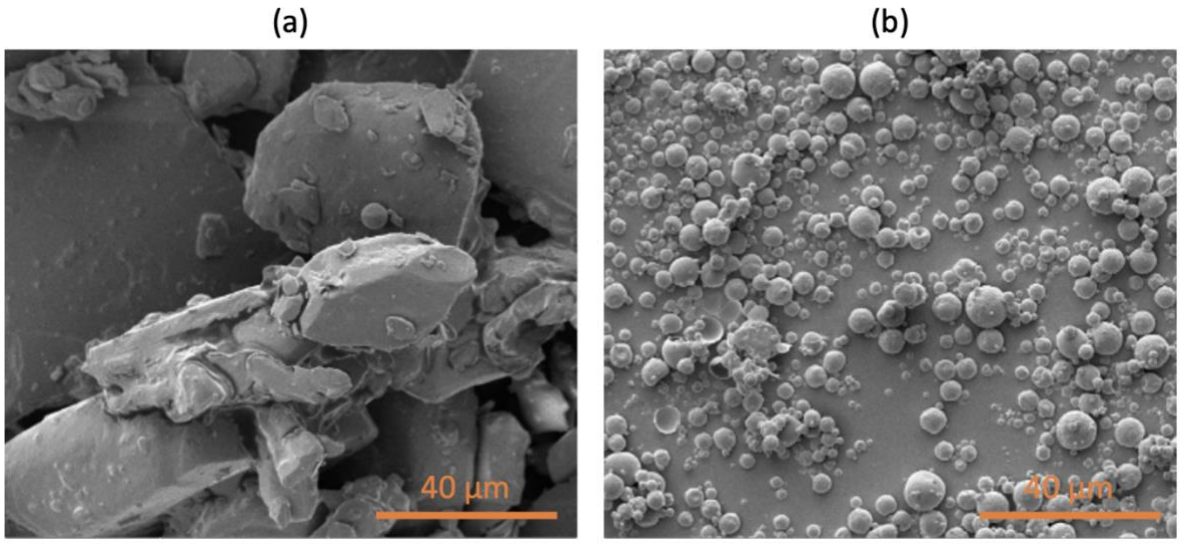

Figure 2. Scanning electron microscopy (SEM) images of (a) L-DOPA crystals and (b) GCPQ-L-DOPA nano-in-microparticles.

SEM analysis of L-DOPA crystals and GCPQ-L-DOPA suggested that both L-DOPA and GCPQ were thoroughly mixed in the GCPQ-L-DOPA microparticles, with no evidence of free L-DOPA

as indicated by the visual absence of L-DOPA crystals in Figure 2b. Furthermore, GCPQ-L-DOPA microparticles had a spherical form, with a non-smooth surface, and a particle size of around 1-20 µm, which corresponds well with the particle size determined via the Malvern Mastersizer.

GCPQ-L-DOPA nano-in-microparticle formulations were also evaluated in terms of drug loading, nanoparticle size, and surface charge after reconstitution of the microparticles in water to achieve a 2 mg mL^{-1} L-DOPA concentration (Table 4). Starting with a GCPQ: L-DOPA mass ratio of 10:2 (17% w/v L-DOPA), a 19.5% w/v L-DOPA content was determined thus, indicating no evidence of L-DOPA degradation during spray drying despite the high temperature (130°C) used.

Table 4. Physicochemical properties of L-DOPA and the GCPQ-L-DOPA 10:2 formulation before and after spray drying (n= 3, mean ± SD, ND = not determined).

Formulation	Z-Average	Peak 1 by size (nm) and intensity (% intensity)	Peak 2 by size (nm) and intensity (% intensity)	Zeta potential (mV)	PDI
GCPQ-L-DOPA before spray drying	76.0 ± 11.0	264 ± 36 (68 ± 6%)	26 ± 4 (29 ± 5%)	ND	0.91 ± 0.17
GCPQ-L-DOPA after spray drying	116.9 ± 17.4	332 ± 30 (74 ± 3%)	35 ± 14 (18 ± 3%)	32.6 ± 8.5	0.93 ± 0.13

As shown in Table 4, reconstitution of GCPQ-L-DOPA nano-in-microparticles generated a mixture of small (28 – 44 nm) and larger (300 – 330 nm) nanoparticles with a highly positive surface charge of +32.6 mV. This particle size distribution is very similar to the one observed with the lyophilised GCPQ-L-DOPA formulations (Table 2). Although there is a small increase in the main peak size, this may be due to the absence of sucrose in the spray-dried formulations. Cryoprotectants such as sucrose improve the dispersibility of formulations and preserve the size of nanoparticles (Zhou, Patel et al. 2013, Wewers, Czyz et al. 2020).

The physical stability of the spray-dried GCPQ-L-DOPA (mass ratio = 10:2) formulations was determined over a 1-month storage period at 4°C and RT by examining key parameters, such as microparticle size, microparticle morphology, drug loading, nanoparticle size, and nanoparticle surface charge. At each timepoint spray-dried formulations were characterised for their microparticle size (Table 5) and morphology (Figure 3) followed by reconstitution in water to measure the remaining parameters (Table 6).

Table 5. Microparticle size distribution stability results of spray-dried GCPQ-L-DOPA (mass ratio = 10:2) nano-in-microparticles stored at 4°C and RT conditions for 1 month (n= 3, mean ± SD).

Formulation (Time)	D_{10} (µm)	D_{50} (µm)	D_{90} (µm)
GCPQ-L-DOPA (0 month)	2.86 ± 0.20	7.16 ± 0.25	15.6 ± 0.6
GCPQ-L-DOPA 4°C (1 month)	2.91 ± 0.18	7.35 ± 0.30	16.0 ± 0.8
GCPQ-L-DOPA RT (1 month)	2.92 ± 0.11	7.26 ±0.27	15.5 ± 0.2

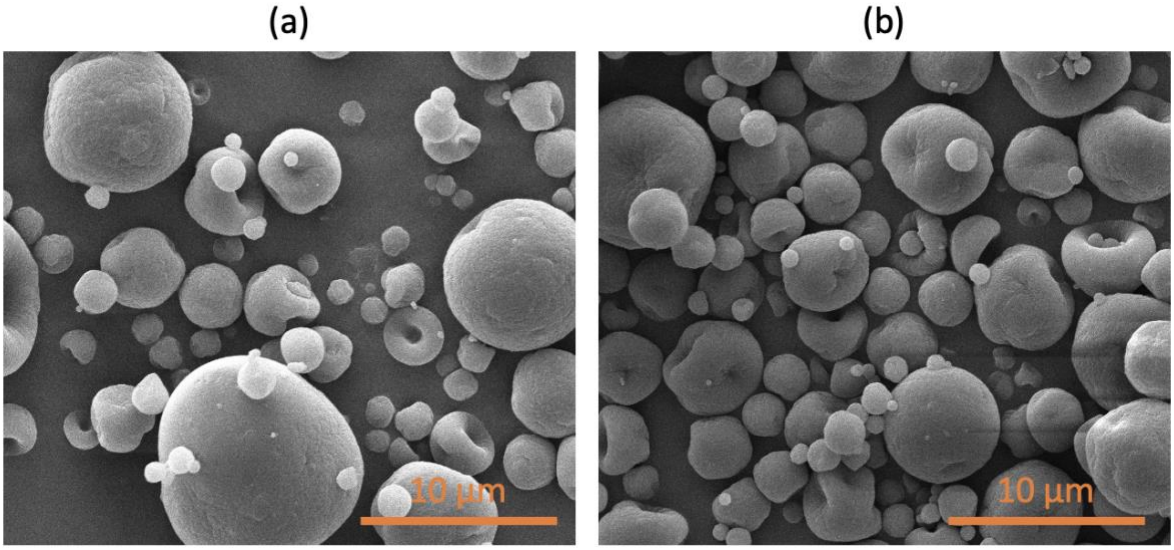

Figure 3. SEM images of spray-dried GCPQ-L-DOPA (mass ratio = 10:2) nano-in-microparticles after 1 month of storage at (a) 4°C and (b) RT conditions.

As shown in Table 5 and Figure 3, the morphology and microparticle size of GCPQ-L-DOPA (mass ratio = 10:2) nano-in-microparticles remained stable for a month regardless of the storage conditions. GCPQ-L-DOPA microparticles were spherical, with a non-smooth surface similar to our earlier findings for other GCPQ microparticles (Godfrey, Iannitelli et al. 2018).

Table 6. Stability results of spray-dried GCPQ-L-DOPA (mass ratio = 10:2) nano-in-microparticles stored at 4°C and RT conditions for 1 month (n= 3, mean ± SD) after reconstitution in aqueous media.

Formulation (Time)	L-DOPA concentration (mg mL^{-1}) and encapsulation efficiency	Z-average (nm)	Peak 1 by size (nm) and intensity (% intensity)	Peak 2 by size (nm) and intensity (% intensity)	Zeta potential (mV)	PDI
GCPQ-L-DOPA (0 month)	7.43 ± 0.18 (93%)	100.7 ± 12.1	380.9 ± 21.9 (72 ± 1%)	40.4 ± 2.7 (21 ± 2%)	40.1 ± 2.5	0.91 ± 0.03
GCPQ-L-DOPA 4°C (1 month)	7.32 ± 0.18 (92%)	105.6 ± 15.2	286.0 ± 6.0 (67 ± 3%)	40.6 ± 3.0 (26 ± 2%)	45.6 ± 3.7	0.92 ± 0.04
GCPQ-L-DOPA RT (1 month)	7.34 ± 0.14 (92%)	113.3 ± 19.9	306.5 ± 41.1 (67 ± 4%)	43.2 ± 12.7 (26 ± 3%)	46.4 ± 2.5	0.89 ± 0.06

GCPQ was able to maintain L-DOPA stably encapsulated at all storage conditions with no reduction in L-DOPA loading (Table 6). Resuspended formulations presented a bimodal particle size distribution with a main peak at 286 – 381 nm (67-72% of the intensity), a secondary peak at 40 – 43 nm (21-26% of the intensity), and a highly positive surface charge (>40 mV) for up to 1 month regardless of the storage conditions.

To date, nano-in-microparticle formulations of L-DOPA for intranasal delivery have not been reported. Microparticles are able to form a system of continuous drug release and thus protect drugs from enzymatic degradation (Pandey, Gadeval et al. 2020). Furthermore, microparticles, capable of adsorbing moisture, become hydrated after absorbing water from epithelial cells and thus, as cells are reversibly dehydrated, junction opening, and drug absorption are promoted (Kulkarni, Bari et al. 2016, Rassu, Ferraro et al. 2018). We have previously shown that intranasally administered reconstituted GCPQ-LENK nano-in-microparticles delivered the peptide exclusively to the brain with no peripheral exposure (Godfrey, Iannitelli et al. 2018). In addition, intranasally administered chitosan microparticles loaded with diltiazem were effective at a 5-fold lower dose in rodents compared to oral treatments (Kulkarni, Bari et al. 2016). Here, we hypothesise that the intranasal administration of the GCPQ-L-DOPA microparticle formulation could reduce peripheral levels of DA and eliminate the drawbacks associated with oral L-DOPA administration. Furthermore, based on the mucoadhesive properties of GCPQ, a controlled release system providing significant levels of DA in the brain could be achieved.

Nasal dosage forms need to agree with regulatory guidelines to be approved for clinical use. Regarding particle size requirements, the target particle size for deposition in the nasal cavity is 10 µm mass-median aerodynamic diameter (MMAD), whereas a more acceptable particle size range is between 4.8 and 23 µm (Leitner, Guggi et al. 2004, Shekunov, Chattopadhyay et al. 2007). Although here we show a smaller microparticle size distribution (Table 5); it is our opinion that with appropriate adjustment of the spray dryer settings, as conducted for GCPQ-LENK (Godfrey, Iannitelli et al. 2018), the recommended particle size could easily be obtained without use of excipients.

3.3. Pharmacokinetics

Crystal L-DOPA and GCPQ-L-DOPA formulations at 1.2 mg kg^{-1} dose were given intranasally to male Sprague Dawley rats and the levels of L-DOPA and DA in plasma and brain were measured. The L-DOPA pharmacokinetics in plasma after the intranasal administration of GCPQ-L-DOPA nanoparticles is shown in Figure 4a, while the L-DOPA plasma levels at the T_{max} (0.25 hours) after intranasal administration of a dispersion of crystalline L-DOPA and GCPQ-L-DOPA nanoparticles (comparative study) at the same intranasal dose (1.2 mg kg^{-1}) is shown in Figure 4b. The L-DOPA concentrations between Figure 4a and 4b are not identical as they are derived from a different set of samples and were separate experiments. The complete L-DOPA pharmacokinetics in plasma after the intranasal administration of crystal L-DOPA and GCPQ-L-DOPA at 1.2 mg kg^{-1} dose appear in the Supplementary Information (Figure S6).

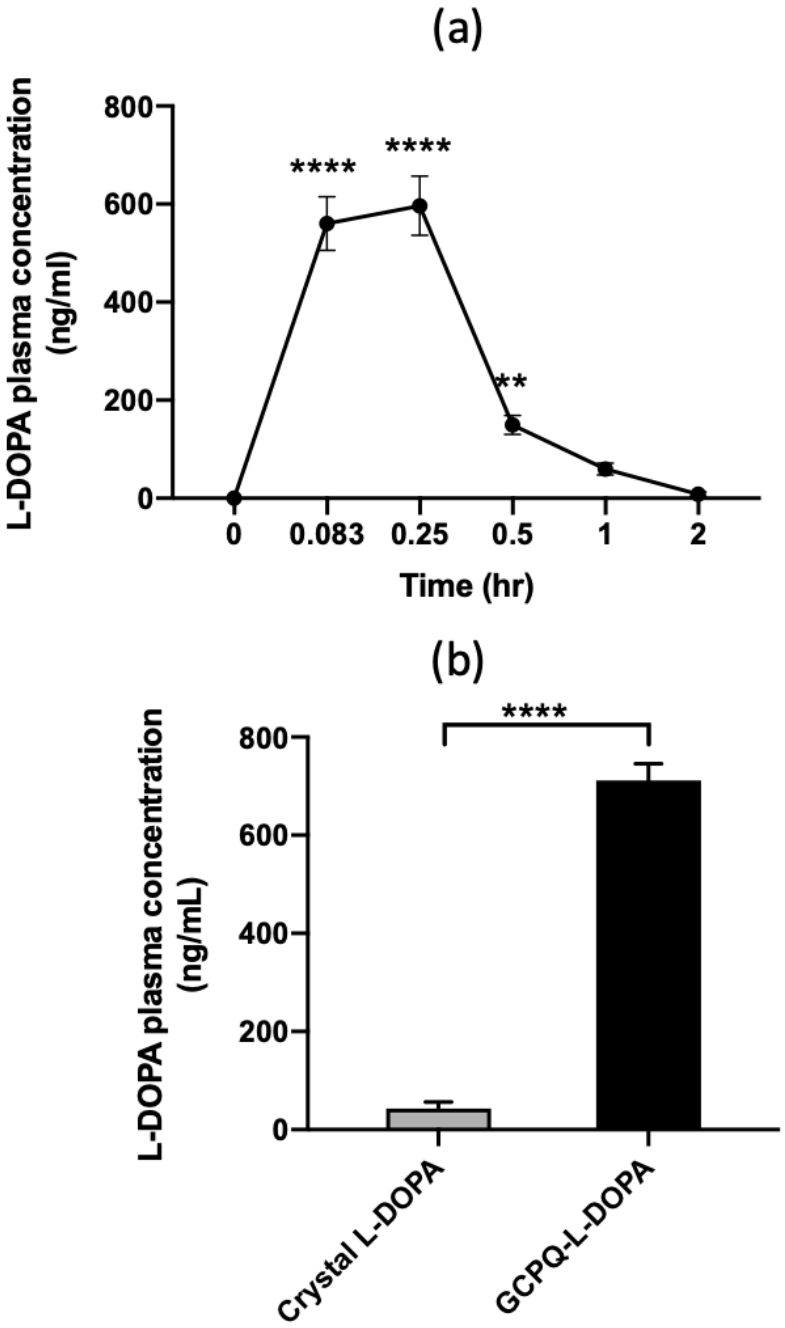

Figure 4. (a) L-DOPA pharmacokinetics in plasma following intranasal administration of GCPQ-L-DOPA at a dose of 1.2 mg kg^{-1} (-•-). Data are expressed as mean ± SEM (n =6-18). Statistical significance of differences for each timepoint compared with t_0 was analysed by Kruskal-Wallis test, followed by Dunn's multiple comparison test (**p < 0.01; ****p < 0.0001). (b) L-DOPA concentration in plasma at T_{max} (0.25 hours) following intranasal administration of crystal L-DOPA and GCPQ-L-DOPA (1.2 mg kg^{-1}). Data are expressed as mean ± SEM (n =5). Statistical significance between both groups was analysed by two-tailed unpaired Student's t test (****p < 0.0001). Values that were below LOQ were computed as 0 for graphing and statistical analysis purposes.

Following intranasal dosing of a dispersion of crystalline L-DOPA, maximum plasma concentrations (53.5 ± 22.7 ng mL^{-1}) of L-DOPA were observed 0.25 hours post-dosing. As the plasma level of L-DOPA was below the limit of quantification in 1 out of 4, 1 out of 4, 1 out of 3 and 2 out of 3 animals at the 0.083-, 0.025-, 1- and 2-hour timepoints respectively, the mean half-life or mean AUC of L-DOPA in plasma could not be determined in these animals. With respect to DA, 22 out of 25 samples at various timepoints returned values that were below the limit of quantification with only single animals within a group of four animals at any timepoint recording a value for DA of 25 – 29 ng mL^{-1}. We conclude that intranasal L-DOPA alone results in non-therapeutic levels of DA in rat plasma samples.

Following intranasal dosing of GCPQ-L-DOPA, maximum plasma concentrations (mean of 711.8 ± 75.4 ng mL^{-1}) of L-DOPA were observed 0.25 hours post-dosing. The mean half-life was 0.427 hours, the $AUC_{0\text{-}Xhr}$ of L-DOPA was 343 ± 3.69 hr ng mL^{-1}, and the mean dose-normalized AUC_{last} was 286 ± 3.07 hr kg ng mL^{-1} mg^{-1}. Regarding DA, the plasma concentrations were below the limit of quantification in all samples apart from one rat (t = 0.083 hours, 25.4 ng mL^{-1}); therefore, no pharmacokinetic parameters could be determined.

Sato *et al* reported a basal level of 2.1 ± 0.6 ng mL^{-1} for L-DOPA (Sato, Koitabashi et al. 1994) and Nedorubov *et al* reported a basal level of 1.71 ± 0.63 ng mL^{-1} for DA in rat plasma (Nedorubov, Pavlov et al. 2018). In our study, we were not able to measure the endogenous plasma concentrations of L-DOPA and DA due to the sensitivity of the LC-MS method (limit of quantification = 5 ng mL^{-1} and 25 ng mL^{-1} for L-DOPA and DA respectively). Furthermore, rats were fasted overnight which could result in much lower endogenous L-DOPA levels in plasma (Ravenstijn, Drenth et al. 2012). Nevertheless, basal L-DOPA plasma levels (< 5 ng mL^{-1}) are negligible when compared with the levels obtained after intranasal administration of GCPQ-L-DOPA in our study.

Interestingly, when L-DOPA is formulated with GCPQ, a ~17-fold increase in L-DOPA plasma concentration was observed at the T_{max} compared to the crystal L-DOPA formulation (Figure 4b). Thus, GCPQ particles appear to transport L-DOPA to the blood more efficiently. L-DOPA is present in the periphery after intranasal administration in many other studies (Kao, Traboulsi et al. 2000, Kim, Kang et al. 2009, Nedorubov, Pavlov et al. 2018). Nevertheless,

without a decarboxylase inhibitor, such as carbidopa, only 1% of peripheral L-DOPA can reach the brain as the drug Is being rapidly converted to DA by the enzyme amino acid decarboxylase (Kim, Kang et al. 2009). Furthermore, intranasal administration of L-DOPA formulated with GCPQ did not contribute significantly to DA plasma levels (values were largely below the limit of quantification). This could be due to the rapid rate of elimination of DA and the slow rate of metabolism of L-DOPA in plasma (Kao, Traboulsi et al. 2000). Therefore, we show here that by not using the oral route, and hence avoiding gastrointestinal wall and hepatic metabolism, we produce substantially lower plasma concentrations of DA. Since the debilitating side effects of oral L-DOPA therapy, such as nausea, tremors, and stiffness, are attributed to higher DA levels in the peripheral circulation (Sasahara, Nitanai et al. 1980), nasal administration of GCPQ-L-DOPA may minimise these adverse effects by not elevating DA concentrations in the blood.

Regarding pharmacokinetics in the brain, all L-DOPA concentrations were below the limit of quantification (50 ng mL^{-1}). Nedorubov *et al* reported a basal level of 3.4 ± 0.9 ng g^{-1} and a C_{max} of 16.94 ± 1.52 for L-DOPA in rat brain tissue after intranasal L-DOPA administration (Nedorubov, Pavlov et al. 2018). Thus, it is possible that we were not able to measure L-DOPA brain levels throughout the study due to the sensitivity of the LC-MS method. Nevertheless, our DA basal levels were 96.3 ng g^{-1}, similar to values obtained in the literature (99.18 ± 20.5 ng g^{-1})(Nedorubov, Pavlov et al. 2018). The DA pharmacokinetics (DA levels in excess of basal levels) in the brain after intranasal administration of GCPQ-L-DOPA and the comparison of the DA brain levels following crystal L-DOPA or GCPQ-L-DOPA intranasal administration (comparative study) at T_{max} (2 hours) are shown in Figure 5a and Figure 5b respectively. The DA concentrations between Figure 5a and 5b are not identical as they are derived from a different set of samples and were separate experiments. All brain levels are reported after subtraction of basal brain levels.

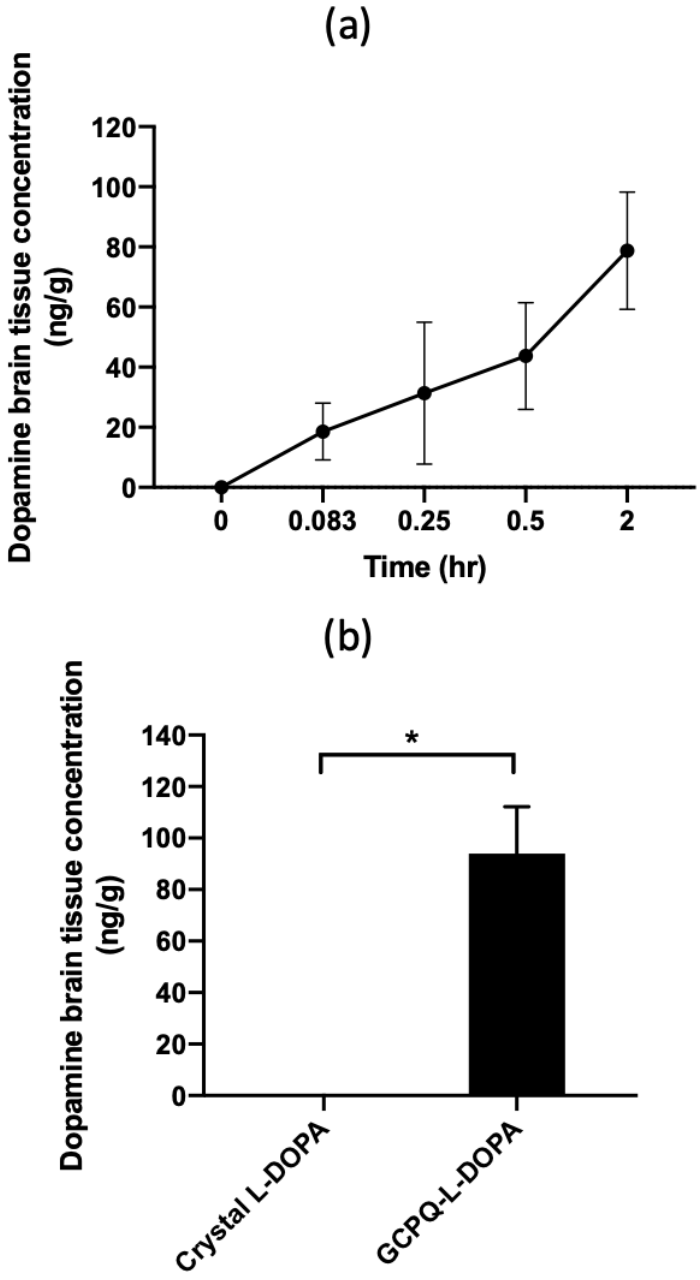

Figure 5. (a) DA pharmacokinetics in brain tissue following intranasal administration of GCPQ-L-DOPA at a dose of 1.2 mg kg^{-1} (-•-). Data are expressed as mean ± SEM (n = 1-6). Differences between each timepoint and t_0 did not reach statistical significance (analysed by ordinary one-way ANOVA, followed by Dunnett's multiple comparison test) (b) DA concentration in brain tissue at T_{max} (2 hours) following intranasal administration of crystal L-DOPA and GCPQ-L-DOPA (1.2 mg kg^{-1}). Data are expressed as mean ± SEM (n =3). Statistical significance between both groups was analysed by two-tailed unpaired Student's t test with Welch's correction (*$p < 0.05$). Measured brain tissue basal levels of DA (96.3 ng g^{-1}) were subtracted from the analysis. Values that were below LOQ were computed as 0 for graphing and statistical analysis purposes.

Although we were not able to detect L-DOPA levels in the brain, we did obtain an increase in the DA brain levels after intranasal administration of GCPQ-L-DOPA with maximum brain concentrations (mean of 94 ± 31.5 ng g^{-1} above the basal levels) of DA observed 2 hours post-dosing. Nedorubov *et al* reported that DA was found in more significant concentrations in rat brains than its precursor, L-DOPA, after intranasal delivery of 3.4 mg kg^{-1} L-DOPA (Nedorubov, Pavlov et al. 2018) compared to 1.2 mg kg^{-1} of our formulated L-DOPA. Interestingly, the crystal L-DOPA formulation did not result in an increase of DA levels in the brain; in fact, DA brain levels following the administration of crystalline L-DOPA suspensions, were below the limit of quantification (Figure 5b). From this we can conclude that the intranasal administration of L-DOPA alone does not yield the pharmacologically relevant levels of DA. On the other hand, when L-DOPA is formulated with GCPQ, it leads to a statistically significant increase in DA concentrations in the brain above the basal levels. The brain DA C_{max} (94 ± 31.5 ng g^{-1}) obtained with the intranasally administered GCPQ-L-DOPA is probably attributed to both nasal cavity-blood circulation-brain pathway as well as the direct nose-to-brain route of L-DOPA and we are unable to distinguish between both delivery routes in this study. There is evidence in the literature that show a transport from the nasal mucosa to the olfactory bulb, and the cerebrospinal fluid (CSF) (Kao, Traboulsi et al. 2000). Preferential absorption of intranasally administered compounds into the olfactory bulb or the CSF has been widely reported (Anand Kumar, David et al. 1982, Sakane, Akizuki et al. 1991, Sakane, Akizuki et al. 1991, Chou and Donovan 1997). Furthermore, we have previously shown direct nose-to-brain delivery using GCPQ nanoparticles (Godfrey, Iannitelli et al. 2018). Nevertheless, the nasal cavity is highly vascularised with many arteries supplying blood to the nasal cavity (Romeo, deMeireles et al. 1998). Therefore, the increased L-DOPA levels in the plasma after intranasal administration of GCPQ-L-DOPA (C_{max} of 711.8 ng mL^{-1}) may contribute substantially to the generation of DA in the brain by L-DOPA absorption through the nasal cavity-blood circulation-brain route.

Interestingly, DA levels keep increasing after 2 hours post-dosing in our study. We speculate that the mucoadhesive properties of our GCPQ particles may enhance the retention time of L-DOPA in the nares and enable a controlled release system, leading to a stable increase in DA levels over the two-hour time period (Figure 5a). Thus, the DA increase that we observe here is attributed to GCPQ-mediated delivery of L-DOPA to the brain via a direct (nose-to-brain) and indirect (nasal cavity-blood circulation-brain) pathway. Although L-DOPA is

detected in the plasma when administered as L-DOPA alone, it barely converts to DA in the brain when not encapsulated in nanoparticles. This demonstrates that nanoparticles facilitate L-DOPA delivery to the brain and effective DA production after enzymatic conversion. Further experiments with a higher intranasal dose and with later timepoints are needed to further support the current findings. Finally, a more sensitive LC-MS method for L-DOPA detection in the brain tissue would allow us to monitor the DA precursor's nose-to-brain delivery more effectively.

From this rat data we conclude that GCPQ-L-DOPA when administered intranasally results in DA formation in the brain with little to no plasma exposure of DA. This should improve the tolerability of DA. Peripheral conversion of L-DOPA to DA appears to be minimal when L-DOPA is administered intranasally in rats without co-administering a peripheral decarboxylase inhibitor.

4. Conclusions

In summary, we utilise GCPQ to stably encapsulate L-DOPA into a nano-in-microparticle formulation at a drug content of 19.5% (w/w). The nano-in-microparticle L-DOPA formulation (D_{10}: 2.86 µm, D_{50}: 7.16 µm and D_{90}: 15.6 µm), with accompanying stability data, gives rise to GCPQ-L-DOPA nanoparticles upon reconstitution. Nasal administration of the reconstituted GCPQ-L-DOPA nano-in-microparticles to rats resulted in DA concentrations steadily increasing in the brain over time (C_{max} of 94 ng g^{-1}, 2 hours post-dosing) with significantly higher levels achieved compared to a crystalline L-DOPA dispersion (below the level of detection, 2 hours post-dosing). This provides evidence of enhanced drug retention in the nares and effective delivery (direct; nose-to-brain and indirect; nasal cavity- blood circulation-brain) through a GCPQ-enabled controlled release system. In addition, nasal administration of GCPQ-L-DOPA resulted in increased L-DOPA availability in plasma (~17-fold increase compared to crystal L-DOPA 15 minutes post-dose), accompanied by insignificant formation of DA in the circulation. The latter suggests that our delivery system could avoid the side effects associated with oral L-DOPA therapy that normally result from increased blood levels of DA. Since the brain is the intended site of action of L-DOPA therapy, the brain targeting achieved by the administration of GCPQ-L-DOPA via the nasal route may provide a safer and thus more efficacious treatment for people with Parkinson's disease.

Acknowledgements

Imbrium Therapeutics and Nanomerics Ltd are acknowledged for funding this study.

Appendix. Supplementary material

The following are the Supplementary data to add to this article:

Table S.1. Assay validation parameters for the quantification of L-DOPA content by HPLC.

Figure S.1. LC-MS/MS spectra of (a) L-DOPA at a 1000 ng mL^{-1} (b) DA at a 1000 ng mL^{-1} and (c) L-DOPA-d_3 at 1000 ng mL^{-1} used to construct the plasma calibration curve after extraction from rat plasma samples.

Figure S.2. LC-MS/MS spectra of (a) L-DOPA at a 1000 ng mL^{-1} (b) DA at a 1000 ng mL^{-1} and (c) L-DOPA-d_3 at 1000 ng mL^{-1} used to construct the brain calibration curve after extraction from rat brain homogenate samples.

Figure S.3. LC-MS/MS spectra of L-DOPA (spiked with 1 µg mL^{-1} of L-DOPA-d_3) of a rat plasma sample from the rat pharmacokinetics study at T = 0.25 hours after intranasal administration of GCPQ-L-DOPA at 1.2 mg kg^{-1}.

Figure S.4. LC-MS/MS spectra of DA (spiked with 1 µg mL^{-1} of L-DOPA-d_3) of a rat brain homogenate sample from the rat pharmacokinetics study at T = 2 hours after intranasal administration of GCPQ-L-DOPA at 1.2 mg kg^{-1}.

Figure S.5. Dynamic light scattering (DLS) analysis of the GCPQ polymer before lyophilisation, and GCPQ-L-DOPA nanoparticles before and after lyophilisation.

Figure S.6. L-DOPA pharmacokinetics in plasma following intranasal administration of crystal L-DOPA and GCPQ-L-DOPA at a dose of 1.2 mg kg^{-1}. Data are expressed as mean ± SEM (n =1-6). Statistical significance between both groups at each timepoint was analysed by a mixed-effects analysis, followed by Sidak's multiple comparisons test (**$p < 0.01$; ****$p < 0.0001$).

References

Abbott, A. (2010). "Levodopa: the story so far." Nature **466**(7310): S6-7.

Abbott, N. J. (2013). "Blood-brain barrier structure and function and the challenges for CNS drug delivery." J Inherit Metab Dis **36**(3): 437-449.

Anand Kumar, T. C., G. F. David, A. Sankaranarayanan, V. Puri and K. R. Sundram (1982). "Pharmacokinetics of progesterone after its administration to ovariectomized rhesus monkeys by injection, infusion, or nasal spraying." Proc Natl Acad Sci U S A **79**(13): 4185-4189.

Arisoy, S., O. Sayiner, T. Comoglu, D. Onal, O. Atalay and B. Pehlivanoglu (2020). "In vitro and in vivo evaluation of levodopa-loaded nanoparticles for nose to brain delivery." Pharm Dev Technol **25**(6): 735-747.

Blandini, F. and J. T. Greenamyre (1999). "Protective and symptomatic strategies for therapy of Parkinson's disease." Drugs Today (Barc) **35**(6): 473-483.

Brime, B., M. P. Ballesteros and P. Frutos (2000). "Preparation and in vitro characterization of gelatin microspheres containing Levodopa for nasal administration." J Microencapsul **17**(6): 777-784.

Bruschi, M. L., S. B. de Souza Ferreira and J. Bassi da Silva (2020). Chapter 4 - Mucoadhesive and mucus-penetrating polymers for drug delivery. Nanotechnology for Oral Drug Delivery. J. P. Martins and H. A. Santos, Academic Press**:** 77-141.

Chou, K. J. and M. D. Donovan (1997). "Distribution of antihistamines into the CSF following intranasal delivery." Biopharm Drug Dispos **18**(4): 335-346.

Chun, I. K., Y. H. Lee, K. E. Lee and H. S. Gwak (2011). "Design and evaluation of levodopa methyl ester intranasal delivery systems." J Parkinsons Dis **1**(1): 101-107.

Contin, M., R. Riva, F. Albani and A. Baruzzi (1996). "Pharmacokinetic optimisation in the treatment of Parkinson's disease." Clin Pharmacokinet **30**(6): 463-481.

Gabathuler, R. (2010). "Approaches to transport therapeutic drugs across the blood-brain barrier to treat brain diseases." Neurobiol Dis **37**(1): 48-57.

Gao, H. (2016). "Progress and perspectives on targeting nanoparticles for brain drug delivery." Acta Pharmaceutica Sinica B **6**(4): 268-286.

Godfrey, L., A. Iannitelli, N. L. Garrett, J. Moger, I. Imbert, T. King, F. Porreca, R. Soundararajan, A. Lalatsa, A. G. Schätzlein and I. F. Uchegbu (2018). "Nanoparticulate peptide delivery exclusively to the brain produces tolerance free analgesia." Journal of Controlled Release **270**: 135-144.

Haddad, F., M. Sawalha, Y. Khawaja, A. Najjar and R. Karaman (2017). "Dopamine and Levodopa Prodrugs for the Treatment of Parkinson's Disease." Molecules (Basel, Switzerland) **23**(1): 40.

Hamsaraj, K. and S. Ramachandra Murthy Rayasa (1970). "Nanotechnology in Brain Targeting." International Journal of Pharmaceutical Sciences and Nanotechnology **1**(1).

Kao, H. D., A. Traboulsi, S. Itoh, L. Dittert and A. Hussain (2000). "Enhancement of the Systemic and CNS Specific Delivery of L-Dopa by the Nasal Administration of Its Water Soluble Prodrugs." Pharmaceutical Research **17**(8): 978-984.

Kim, T. K., W. Kang, I. K. Chun, S. Y. Oh, Y. H. Lee and H. S. Gwak (2009). "Pharmacokinetic evaluation and modeling of formulated levodopa intranasal delivery systems." Eur J Pharm Sci **38**(5): 525-532.

Kulkarni, A. D., D. B. Bari, S. J. Surana and C. V. Pardeshi (2016). "In vitro, ex vivo and in vivo performance of chitosan-based spray-dried nasal mucoadhesive microspheres of diltiazem hydrochloride." Journal of Drug Delivery Science and Technology **31**: 108-117.
Lalatsa, A., N. L. Garrett, T. Ferrarelli, J. Moger, A. G. Schätzlein and I. F. Uchegbu (2012). "Delivery of Peptides to the Blood and Brain after Oral Uptake of Quaternary Ammonium Palmitoyl Glycol Chitosan Nanoparticles." Molecular Pharmaceutics **9**(6): 1764-1774.
Leenders, K. L., W. H. Poewe, A. J. Palmer, D. P. Brenton and R. S. Frackowiak (1986). "Inhibition of L-[18F]fluorodopa uptake into human brain by amino acids demonstrated by positron emission tomography." Ann Neurol **20**(2): 258-262.
Leitner, V. M., D. Guggi, A. H. Krauland and A. Bernkop-Schnürch (2004). "Nasal delivery of human growth hormone: in vitro and in vivo evaluation of a thiomer/glutathione microparticulate delivery system." J Control Release **100**(1): 87-95.
Maguire, C. M., M. Rösslein, P. Wick and A. Prina-Mello (2018). "Characterisation of particles in solution - a perspective on light scattering and comparative technologies." Science and technology of advanced materials **19**(1): 732-745.
Melamed, E., F. Hefti and R. J. Wurtman (1980). "Nonaminergic striatal neurons convert exogenous L-dopa to dopamine in parkinsonism." Ann Neurol **8**(6): 558-563.
Nedorubov, A. A., A. N. Pavlov, N. V. Pyatigorskaya, G. E. Brkich and Z. Aladysheva (2018). "HPLC-MS/MS method application for the determination of pharmacokinetic parameters of intranasal delivered L-DOPA in rats." Journal of Pharmaceutical Sciences and Research **10**: 2489-2492.
Nedorubov, A. A., A. N. Pavlov, N. V. Pyatigorskaya, G. E. Brkich and M. M. Shabalina (2019). "Pharmacokinetics of Nanosomal Form of Levodopa in Intranasal Administration." Open access Macedonian journal of medical sciences **7**(21): 3509-3513.
Olanow, C. W., M. B. Stern and K. Sethi (2009). "The scientific and clinical basis for the treatment of Parkinson disease (2009)." Neurology **72**(21 Suppl 4): S1-136.
Pandey, V., A. Gadeval, S. Asati, P. Jain, N. Jain, R. Roy, M. Tekade, V. Soni and R. Tekade (2020). Formulation strategies for nose-to- brain delivery of therapeutic molecules**:** 291-332.
Pardeshi, C. V., V. S. Belgamwar, A. R. Tekade and S. J. Surana (2013). "Novel surface modified polymer-lipid hybrid nanoparticles as intranasal carriers for ropinirole hydrochloride: in vitro, ex vivo and in vivo pharmacodynamic evaluation." J Mater Sci Mater Med **24**(9): 2101-2115.
Patel, A. B. and J. Jimenez-Shahed (2018). "Profile of inhaled levodopa and its potential in the treatment of Parkinson's disease: evidence to date." Neuropsychiatr Dis Treat **14**: 2955-2964.
Pires, P. C. and A. O. Santos (2018). "Nanosystems in nose-to-brain drug delivery: A review of non-clinical brain targeting studies." J Control Release **270**: 89-100.
Polanowska, K., R. M. Łukasik, M. Kuligowski and J. Nowak (2019). "Development of a Sustainable, Simple, and Robust Method for Efficient l-DOPA Extraction." Molecules **24**(12).
Pyrć, K., A. Milewska, E. B. Duran, P. Botwina, R. Lopes, A. Arenas-Pinto, M. Badr, R. Mellor, T. L. Kalber, D. Fernandes-Reyes, A. G. Schätzlein and I. F. Uchegbu (2020). "SARS-CoV-2 inhibition in human airway epithelial cells using a mucoadhesive, amphiphilic chitosan that may serve as an anti-viral nasal spray." bioRxiv: 2020.2012.2010.413609.
Qu, X., V. V. Khutoryanskiy, A. Stewart, S. Rahman, B. Papahadjopoulos-Sternberg, C. Dufes, D. McCarthy, C. G. Wilson, R. Lyons, K. C. Carter, A. Schätzlein and I. F. Uchegbu (2006). "Carbohydrate-based micelle clusters which enhance hydrophobic drug bioavailability by up to 1 order of magnitude." Biomacromolecules **7**(12): 3452-3459.

Rassu, G., L. Ferraro, B. Pavan, P. Giunchedi, E. Gavini and A. Dalpiaz (2018). "The Role of Combined Penetration Enhancers in Nasal Microspheres on In Vivo Drug Bioavailability." Pharmaceutics **10**(4): 206.
Rautio, J., H. Kumpulainen, T. Heimbach, R. Oliyai, D. Oh, T. Järvinen and J. Savolainen (2008). "Prodrugs: design and clinical applications." Nature Reviews Drug Discovery **7**(3): 255-270.
Ravenstijn, P. G., H. J. Drenth, M. J. O'Neill, M. Danhof and E. C. de Lange (2012). "Evaluation of blood-brain barrier transport and CNS drug metabolism in diseased and control brain after intravenous L-DOPA in a unilateral rat model of Parkinson's disease." Fluids Barriers CNS **9**: 4.
Romeo, V. D., J. deMeireles, A. P. Sileno, H. K. Pimplaskar and C. R. Behl (1998). "Effects of physicochemical properties and other factors on systemic nasal drug delivery." Adv Drug Deliv Rev **29**(1-2): 89-116.
Sakane, T., M. Akizuki, S. Yamashita, T. Nadai, M. Hashida and H. Sezaki (1991). "The transport of a drug to the cerebrospinal fluid directly from the nasal cavity: the relation to the lipophilicity of the drug." Chem Pharm Bull (Tokyo) **39**(9): 2456-2458.
Sakane, T., M. Akizuki, M. Yoshida, S. Yamashita, T. Nadai, M. Hashida and H. Sezaki (1991). "Transport of cephalexin to the cerebrospinal fluid directly from the nasal cavity." J Pharm Pharmacol **43**(6): 449-451.
Sasahara, K., T. Nitanai, T. Habara, T. Morioka and E. Nakajima (1980). "Dosage form design for improvement of bioavailability of levodopa III: Influence of dose on pharmacokinetic behavior of levodopa in dogs and Parkinsonian patients." J Pharm Sci **69**(12): 1374-1378.
Sato, S., T. Koitabashi and A. Koshiro (1994). "Pharmacokinetic and pharmacodynamic studies of L-dopa in rats. I. Pharmacokinetic analysis of L-dopa in rat plasma and striatum." Biol Pharm Bull **17**(12): 1616-1621.
Seju, U., A. Kumar and K. K. Sawant (2011). "Development and evaluation of olanzapine-loaded PLGA nanoparticles for nose-to-brain delivery: in vitro and in vivo studies." Acta Biomater **7**(12): 4169-4176.
Sharma, S., S. Lohan and R. S. Murthy (2014). "Formulation and characterization of intranasal mucoadhesive nanoparticulates and thermo-reversible gel of levodopa for brain delivery." Drug Dev Ind Pharm **40**(7): 869-878.
Shekunov, B. Y., P. Chattopadhyay, H. H. Y. Tong and A. H. L. Chow (2007). "Particle Size Analysis in Pharmaceutics: Principles, Methods and Applications." Pharmaceutical Research **24**(2): 203-227.
Siew, A., H. Le, M. Thiovolet, P. Gellert, A. Schatzlein and I. Uchegbu (2012). "Enhanced oral absorption of hydrophobic and hydrophilic drugs using quaternary ammonium palmitoyl glycol chitosan nanoparticles." Mol Pharm **9**(1): 14-28.
Stocchi, F., S. Ruggieri, A. Carta, P. Jenner and A. Agnoli (1989). "Different therapeutic approaches in Parkinson's disease. Clinical, pharmacological and physiological aspects." Disorders of movements: 137-146.
Tambasco, N., M. Romoli and P. Calabresi (2018). "Levodopa in Parkinson's Disease: Current Status and Future Developments." Current neuropharmacology **16**(8): 1239-1252.
Tolosa, E., M. J. Martí, F. Valldeoriola and J. L. Molinuevo (1998). "History of levodopa and dopamine agonists in Parkinson's disease treatment." Neurology **50**(6 Suppl 6): S2-10; discussion S44-18.
Wade, D. N., P. T. Mearrick and J. L. Morris (1973). "Active Transport of L-Dopa in the Intestine." Nature **242**(5398): 463-465.
Wang, Z., G. Xiong, W. C. Tsang, A. G. Schätzlein and I. F. Uchegbu (2019). "Nose-to-Brain Delivery." Journal of Pharmacology and Experimental Therapeutics **370**(3): 593.

Wewers, M., S. Czyz, J. H. Finke, E. John, B. Van Eerdenbrugh, M. Juhnke, H. Bunjes and A. Kwade (2020). "Influence of Formulation Parameters on Redispersibility of Naproxen Nanoparticles from Granules Produced in a Fluidized Bed Process." Pharmaceutics **12**(4).
Wu, H., K. Hu and X. Jiang (2008). "From nose to brain: understanding transport capacity and transport rate of drugs." Expert Opin Drug Deliv **5**(10): 1159-1168.
Zahoor, I., A. Shafi and E. Haq (2018). Pharmacological Treatment of Parkinson's Disease**:** 129-144.
Zhou, J., T. R. Patel, R. W. Sirianni, G. Strohbehn, M. Q. Zheng, N. Duong, T. Schafbauer, A. J. Huttner, Y. Huang, R. E. Carson, Y. Zhang, D. J. Sullivan, Jr., J. M. Piepmeier and W. M. Saltzman (2013). "Highly penetrative, drug-loaded nanocarriers improve treatment of glioblastoma." Proc Natl Acad Sci U S A **110**(29): 11751-11756.
zhou, w., C. Liu, F. Yu, X. Niu, X. Wang, G. Li and l. Xinru (2020). Co-loading of Levodopa and Curcumin Using Brain-targeted Protocells as a Drug Delivery System for Improving the Efficacy of Parkinson's Disease.